Revised manuscript-Revision 1

Constraints on the mobilization of Zr in magmatic-hydrothermal processes in subduction zones from *in situ* fluid-melt partitioning experiments

Marion Louvel[1,*,**], Carmen Sanchez-Valle[1,*], Wim J. Malfait[1], Herve Cardon[2], Denis Testemale[3], Jean-Louis Hazemann[3]

[1]Institute for Goechemistry and Petrology, ETH Zurich, CH-8092 - Zurich, Switzerland.
[2]Laboratoire de Géologie de Lyon, ENS Lyon, FR-69364 – Lyon, France.
[3]Institut Néel, Département MCMF-Grenoble, F-38042 - Grenoble, France.

Abstract

The partition of Zr between high P-T aqueous fluids and melts has been investigated *in situ* in the haplogranite-H_2O and haplogranite-(F)-H_2O systems to assess the mobilization of High Field Strength Elements (HFSE) in magmatic-hydrothermal processes in subduction zones. **The partition coefficients $D_{Zr}^{f/m}$ were determined from Zr concentrations measured *in situ* by Synchrotron X-ray Fluorescence (SXRF) in both aqueous fluids and F-free or F-bearing hydrous haplogranite melts equilibrated in diamond-anvil cells at 575 to 800 °C and 0.3 to 2.4 GPa. This experimental approach eliminates the need for internal or external calibrations of the SXRF signal and/or post-mortem analysis of the melt phase, hence decreasing the total uncertainties on $D_{Zr}^{f/m}$ below 16%.** Above 0.6 GPa, Zr partitions favorably into the hydrous silicate melt in both F-free and F-bearing systems, with $D_{Zr}^{f/m}$ that range between 0.19 ± 0.02 and 0.38 ± 0.03. However, **the relatively high $D_{Zr}^{f/m}$ values indicate that alkali-silica rich aqueous fluids generated by metamorphic devolatilization may contribute significantly to the recycling of HFSE in subduction zones.** The efficient uptake of Zr (and likely other HFSE) by subduction zone fluids, regardless of their nature (aqueous fluid,

hydrous melt or supercritical fluid), supports the idea that the typical HFSE depletion recorded in arc magmas does not result from their incompatibility in water-rich slab-derived fluids but most probably originates from complex fluid-melt-rock interactions occurring at the slab interface and within the mantle wedge. At shallow crustal pressure conditions (800 °C and 0.3 GPa), Zr reversely partitions into the aqueous fluid in the presence of fluorine ($D_{Zr}^{f/m}$ = 1.40 ±0.10) as observed for Nb at similar conditions by Webster et al. (1989). The enrichment of the aqueous phase in HFSE (Zr, Nb) at shallow crustal conditions **is likely related to the enhanced peralkalinity of low pressure, F-bearing aqueous fluid with temperature**, that provides the favorable conditions for their mobilization *via* the formation of HFSE-O-Si/Na clusters. This mechanism may control the enrichment in HFSE (and plausibly other rare metals such as REE) in early magmatic fluids exsolved from granitic melts, leading to the formation of HFSE-enriched aggregates in shallow magmatic-hydrothermal environments (*e.g.,* Strange Lake and Thor Lake Nechalacho deposit, Canada; Galineiro complex, Spain).

Keywords: zirconium, HFSE, fluid-melt partition coefficients, SXRF, subduction zones, rare metal deposits

* Corresponding author: marion.louvel@anu.edu.au; carmen.sanchez@erdw.ethz.ch

** Present address: Research school of Earth Sciences, ANU, AU-0200, Canberra, Australia.

1. Introduction

It is widely accepted that volatile-rich fluids released from the subducting slab favor partial melting of the mantle wedge and drive arc magmatism (Hermann et al., 2006; Johnson and Plank, 1999; Manning, 2004; Schmidt and Poli, 1998; Tastumi and Eggins, 1995). However, the link between the chemistry of subduction zone fluids (*e.g.,* aqueous fluid, supercritical liquid or slab melt) and the trace element signature of arc magmas remains poorly understood. Subduction-related volcanic rocks are characterized by a strong enrichment in large ion lithophile elements (LILE: Sr, Rb, Th, U…) and a depletion in high-field strength elements (HFSE: Nb, Ta, Zr, Ti, Hf) compared to mid-ocean ridge basalts (Gill, 1981; Hawkesworth et al., 1991). This signature is mainly controlled by the incompatible or compatible behavior of trace elements upon fluid/melt-rock interactions in the slab and/or the mantle wedge. For instance, the HFSE depletion has commonly been assigned to the low solubility of HFSE-bearing accessory phases, such as rutile or zircon, in H_2O (Antignano and Manning, 2008; Audetat and Keppler, 2005; Tropper and Manning, 2005) and their selective segregation in minerals from the slab or the mantle wedge such as Ti-clinohumite, olivine, pyroxenes, garnet or spinel (Brenan et al., 1994; Foley et al., 2000; Kelemen et al., 1990; Rudnick et al., 2000; Rubatto and Hermann, 2003; Scambelluri and Philippot, 2001; Spandler et al., 2007). This assignment supports a significant contribution of diluted aqueous fluids to mantle wedge metasomatism. **Conversely**, the relative HFSE-enrichment recorded in high-Nb basalts (HNB) or adakitic magmas in volcanic arcs such as Kamtchatcka, Cascades, or Lesser Antilles (Bouvier et al., 2010; Defant and Drummond, 1993; Munker et al., 2004) has frequently been attributed to the contribution of hydrous slab melts to their primary source, in good agreement with the relatively high solubility and partitioning of HFSE in silicic melts (Dickinson and Hess, 1985; Keppler, 1993; Hermann

and Rubatto, 2009; Linnen and Keppler, 1997; Linnen and Keppler, 2002; Klimm et al., 2008). However, the occurrence of rutile or zircon-rich veins in UHP metamorphic rocks (Gao et al., 2007; Rubatto and Hermann, 2003) indicate that high temperature aqueous fluids have the potential to mobilize and transport nominally insoluble HFSE in subduction zones. Experimental studies provide further evidences that the addition of Cl, F and alkali-silicates can significantly enhance the solubility of HFSE-bearing phases in aqueous fluids (Antignano and Manning, 2008; Hayden and Manning, 2011; Manning et al., 2008; Rapp et al., 2010; Wilke et al., 2012), most probably *via* the formation of alkali-silicate complexes (Louvel et al., 2013; Wilke et al., 2012). The aqueous fluids produced by metamorphic devolatilization of the subducting slab can contain up to several wt% of dissolved Si, Na and Cl (Scambelluri and Phillipot, 2001, Manning, 2004). Consequently, melting of the slab may not be required to produce HFSE enrichment of arc magmas. The efficient uptake of HFSE by aqueous fluids is also recorded in large crustal granitic complexes, where remobilization of HFSE by highly alkaline late-magmatic fluids was found to enhance the potential to form economical rare metal ore deposits (Zr, Nb, REE - Strange Lake and Thor Lake Nechalacho deposit, Canada; Galineiro complex, Spain - Agangi et al., 2010; Gysi and Williams-Jones, 2013; Salvi and Williams-Jones, 1996; Sheard et al., 2012).

The goal of this paper is to improve our understanding of the processes controlling the mobilization/segregation of HFSE in subduction zones and their hydrothermal enrichment in large granitic complexes in the shallow crust. This requires better constraints on the partitioning behavior of HFSE in complex fluid-melt-rock systems at relevant pressure and temperature conditions. Up to now, experimental studies of the distribution of HFSE are however mainly limited to investigations of HFSE partitioning between crystals and melts $D^{c/m}$ (Gaetani et al., 2003; Green et al., 2000; Hill et al., 2011; Kelemen et al., 1990; Klemme et al., 2002; Klemme et

al., 2005; Klimm et al., 2008; Prowatke et Klemme, 2005). Very few studies have determined crystal-fluid partitioning coefficients $D^{c/f}$ for HFSE at such conditions (Adam et al., 1997; Ayers et al., 1997; Kessel et al., 2005; Stalder et al., 1998), mostly due to challenges associated to the recovery and analysis of solute-rich fluid phases. In addition, investigations of fluid-melt partitioning of HFSE have been limited to the study of magmatic-hydrothermal processes in the crust (P < 0.3 GPa - Borodulin et al., 2009; Keppler, 1996; London et al., 1988; Webster et al., 1989) without direct applications to assess the mobilization of HFSE from subducting slab. **Measurements of aqueous fluid-melt partition coefficients $D^{f/m}$ at high P-T conditions are advantageous because the equilibration times for melt-fluid systems are shortened compared to crystal-fluid systems. Moreover, the $D^{f/m}$ values can be converted into $D^{c/f}$ values using available $D^{c/m}$ data according to the equation $\boldsymbol{D^{c/f} = D^{c/m}/D^{f/m}}$.**

In this contribution, we present *in situ* experiments conducted to investigate the partition of Zr between aqueous fluids and silicate melts at P-T conditions **relevant for subduction zones and crustal magmatic-hydrothermal settings**. Fluid-melt partition coefficient of Zr ($D_{Zr}^{f/m}$) were determined from *in situ* Synchrotron X-ray Fluorescence (SXRF) analysis of **alkali silicate-bearing** aqueous fluids and hydrous haplogranitic (F-free and F-bearing) melts equilibrated in hydrothermal diamond-anvil cells (HDAC - Bassett et al., 1993) at 575 °C to 800 °C and 0.3 to 2.4 GPa. **The *in situ* characterization of both the aqueous fluid and hydrous melt phases overcomes the need for calibrations of the absolute fluorescence signal, the use of internal standards or *post-mortem* analysis of the quenched hydrous melts, hence reducing total uncertainties in $D_{Zr}^{f/m}$ below 16%. The investigated haplogranitic melts are peralkaline in composition and represent reasonable analogs for slab melts produced by the breakdown of alkali-rich phases (*i.e.*, phengite, biotite or amphiboles) during the**

hydrous melting of subducted pelite or MOR-basalts (Hermann and Spandler, 2008; Prouteau et al., 2001), and for the composition of granitic bodies that lead to the formation of HFSE deposits in the upper crust (Salvi and Williams-Jones, 1996; Montero et al., 1998). The results are used to discuss the role of aqueous phases in the transport and deposition of Zr, and by extension other HFSE, in subduction-related metamorphic and magmatic environments, from the subducting slab to the upper crust.

2. METHODS

2.1. *In situ* SXRF measurements in the HDAC

The partition of Zr between haplogranite melts and aqueous fluids was investigated as a function of pressure, temperature and composition in high P-T experiments conducted in Bassett-type hydrothermal diamond-anvil cells (HDAC - Bassett et al., 1993). The HDAC were mounted with low fluorescence type Ia diamonds with a 600 or 700 μm diameter culet. The thickness of the diamond window on the detector side was reduced to 1.2 mm to decrease the detection limits of the SXRF analysis (Sanchez-Valle et al., 2004). The sample chamber was formed by a 300 μm hole drilled in a 250 μm thick rhenium gasket compressed between the two diamond anvils and externally heated with Mo wires wrapped around the WC seats supporting the diamond anvils. During heating, the cell was continuously flushed with a reducing gas (98 % Ar - 2 % H mixture) to prevent the oxidation of the Mo heaters, the WC seats or the diamond anvils. Temperature was measured to ±2 °C with K-type thermocouples attached on each diamond-anvil near the sample chamber. The temperature gradient between the thermocouples and the sample chamber was calibrated for each HDAC using the melting temperature at ambient pressure of sulphur (115.4 °C), sodium nitrate (308 °C) and sodium chloride (800.5 °C). The pressure in the sample

chamber was monitored with a precision better than 10% from the variation of the lattice parameters of an Au internal pressure standard determined by angle-dispersive X-ray diffraction (Louvel et al., 2013) using the equation of state for Au of Jamieson et al. (1982).

The sample chamber was loaded with a piece of Zr-bearing haplogranite glass and a pellet of a mixture of Au + Al_2O_3 powders used for pressure calibration (Louvel et al., 2013) and subsequently filled with Milli-Q water. Fluorine-free and fluorine-bearing haplogranite glasses, both doped with 4000 ppm Zr, were used in the experiments to determine the influence of F on the partition of Zr between aqueous fluids and melts (Table 1). The haplogranite glass samples are from the same batch used in a previous study of the speciation of Zr in subduction zone fluids and details about the synthesis and characterization are found in Louvel et al. (2013). The volumetric proportions of glass and aqueous fluid in the loading were adjusted by adding double-side polished glass pieces of known proportions to the **sample chamber of known dimensions.** Upon heating and compression, the haplogranite melt-aqueous fluid system display the phase relations documented in previous studies (*e.g.,* Bureau and Keppler, 1999; Mibe et al., 2008; Shen and Keppler, 1995). Depending on pressure conditions, hydrous melting of the haplogranite glass was observed at around 600-650 °C. The partitioning measurements were performed in the coexisting hydrous melt and aqueous fluid up to 800 °C (Table 2). A microphotograph of the sample chamber arrangement during the experiments can be found in Fig. 1.

SXRF measurements were performed at the BM30b – FAME beamline of the European Synchrotron Radiation Facility (ESRF - Grenoble, France – Proux et al., 2005-2006) together with the X-ray absorption spectroscopy (XAS) measurements previously reported in Louvel et al. (2013). Briefly, SXRF spectra were collected using a monochromatic beam of 18.05 keV focused down to 10 x 15 μm^2 (FWMH VxH) by a set of Kirkpatrick-Baez mirrors. This

configuration ensured a photon flux of ~ 10^9 photons/s at the Zr K-edge energy. The emitted fluorescence radiation (Zr Kα = 15.77 keV) was collected in transmission at the rear-side of the cell using a Si drift detector set at 20° from the incident beam in the horizontal plane (Sanchez-Valle et al., 2003; 2004). This configuration enables collecting SXRF throughout the entire sample chamber and hence the *in situ* sampling of both the aqueous fluid and the hydrous melt at identical P-T conditions (Fig. 2.), with the advantage of avoiding *post-mortem* characterization of the quench melt (Bureau et al., 2007; Borchert et al., 2009). Angle-dispersive X-ray diffraction patterns (λ = 0.69654 Å) were collected on the internal Au pressure calibrant before and after each SRXF analysis using a high-resolution CCD camera positioned behind the cell in transmission geometry.

After each heating step, the temperature was stabilized for about 30 min. The temporal evolution of the Zr concentration in the fluid and hydrous melt was monitored by repeated SXRF analysis in both phases until the intensity of the fluorescence signal (*i.e,* Zr concentration) was constant. **Equilibrium was typically achieved within less than 30 minutes after reaching the target P-T conditions, in agreement with previous reports (Borchert et al., 2009).** 2D-SXRF concentration maps and transversal fluorescence scans were collected across the sample chamber to monitor the distribution of Zr between the aqueous and melt phases (Fig. 1). Careful attention was given that the system reached a stable state where the melt globule was stationary and bridging both diamonds to ensure the sampling of pure fluid and melt phases without contamination of the signal from the coexisting phase (Fig. 2 and 3). A minimum of three fluorescence spectra were collected in several locations across the fluid and the melt phases with counting times of 30 s. The intensities of spectra collected in each phase at identical P-T conditions were constant within < 5%, indicative of the homogeneity of the fluid and melt

186 phases. All SXRF spectra were normalized to the incident beam intensity for the quantitative
187 analysis. Characteristic normalized fluorescence spectra recorded in the aqueous fluid and
188 silicate melt at high P-T are reported in Fig. 3.
189
190 **2.2. Determination of fluid-melt partition coefficients $D_{Zr}^{fluid/melt}$**
191 The integrated intensity of the X-ray fluorescence emission line of an element (I_i) and its
192 concentration in the analyzed phase (C_i) are related through a complex expression that depends
193 on element-related factors (fluorescence cross section), experiment-related factors (angle of
194 detection, contribution of the different media traversed by the X-ray) and sample-related factors
195 such as density or thickness (Cauzid et al., 2006; Sanchez-Valle et al., 2004; Sparks, 1980). It
196 can be reduced as:

197 $$I_i = I_0 * t * A_{eff} * e^{-B} * e^{-C} * C_i * \sigma_i \rho_s * e^{-X} \quad (1)$$

198
199 where I_0 is the intensity of the incoming beam; t is the counting time; A_{eff} accounts for the
200 efficiency of the fluorescence detector at the energy of the emitted signal; σ_i is the fluorescence
201 cross section of the element *i* at the incident energy E_0 and ρ_s is the density of the sample. The
202 parameters B, C and X are correction factors taking into account the absorption coefficient, the
203 density and the thickness of the different media (*i.e.* air, diamond and sample) traversed by the
204 X-rays and the geometry of the experimental set-up. As the partition coefficient of Zr between
205 the fluid and melt phase, $D_{Zr}^{f/m}$, corresponds to the ratio between the concentrations of Zr in each
206 phase, equation (1) can be rearranged as:

207 $$D_{Zr}^{f/m} = \frac{C_{Zr}^f}{C_{Zr}^m} = \frac{\frac{I_{Zr}^f}{\rho_f * e^{-X_f}}}{\frac{I_{Zr}^m}{\rho_m * e^{-X_m}}} \quad (2)$$

where all the terms that account for the experimental set-up (*e.g.,* geometry and presence of different media on the path from the sample to the detector) and normalized counting times cancel out as they are identical for the spectra collected in the fluid and melt phase at given P-T conditions. Therefore, the emitted signal only has to be corrected for the different density and X-ray transmission of the fluid and melt phases. The terms e^{-Xi} represent the effective transmission of the signal through the fluid (f) or the melt (m) phases (hereafter referred to as $\mathbf{T^f_{eff}}$ **and** $\mathbf{T^m_{eff}}$) that depend on the composition, density and thickness of each phase. Therefore, $D_{Zr}^{f/m}$ is obtained from the experimental spectra as:

$$D_{Zr}^{f/m} = \frac{I_{Zr}^{f}}{I_{Zr}^{m}} * \frac{\boldsymbol{T_{eff}^{m}}}{\boldsymbol{T_{eff}^{f}}} * \frac{\rho_m}{\rho_f} \quad (3)$$

where I^f and I^m are the integrated intensity of the normalized fluorescence line as determined after background removal using a standard peak-fitting routine included in Peakfit v4.12 software (SeaSolve Software-USA). The high quality of all collected spectra and the possibility of resolving the fluorescence line of Zr without overlapping with other emission lines reduce the errors in the integrated intensity ratios (Fig. 3), with standard deviations that typically do not exceed 10 % (Table 2). ρ_f and ρ_m are the fluid and melt densities at the relevant pressures, temperatures and phase compositions (Table 2).

228

229 **2.3. Fluid composition, absorption corrections and associated uncertainty on $D_{Zr}^{f/m}$**

230 The composition of the aqueous fluid and coexisting hydrous silicate melt at high P-T,
231 *i.e.,* the amount of dissolved silicates (as total silicates including SiO_2, Na_2O, K_2O and Al_2O_3
232 oxides) in the fluid and the H_2O content in the hydrous melt, could not be determined *in situ* in
233 the present experiments due to the inaccessibility of their absorption edges for SXRF analysis in
234 the diamond anvil cell (*e.g.,* Bassett et al., 2000, Sanchez-Valle, 2013). Consequently, the
235 equilibrium phase compositions and associated densities at high P-T were determined from
236 available experimental data on related compositions and P-T conditions (*e.g.,* Anderson and
237 Burnham, 1983; Driesner and Heinrich, 2007; Malfait et al., 2013; Mantegazzi et al., 2013;
238 Mysen and Wheeler, 2000; Wohlers et al., 2011). The recourse to data on related compositions
239 results in larger associated uncertainties in the derived partition coefficients that have been
240 assessed taking into account additional experimental uncertainty on the pressure calibration (10
241 %). The calculated compositions and densities for all investigated P-T conditions are reported in
242 Table 2 together with the associated uncertainties.

243 The total amount of solutes dissolved in the aqueous fluid at each P-T condition was
244 calculated by extrapolating data on the solubility of albite by Anderson and Burnham (1983) to
245 our experimental P-T conditions and taking into account the retrograde solubility with pressure
246 reported by Wohlers et al. (2011) at 600 °C. These calculations yield between 1.1 ± 0.2 and 15.5
247 ± 2.8 wt% silicates dissolved in the aqueous fluid phase at the investigated conditions (Table 2).
248 At the higher pressure investigated (> 1 GPa and 600 °C), a range of solute contents is proposed
249 to account for uncertainties in the calculations due to the lack of solubility data at appropriated
250 pressure conditions. **The composition of the high pressure hydrous melts is more difficult to**

assess. LA-ICMPS analyses conducted on the quench melt globules show that the hydrous melt equilibrated with the aqueous phase at high pressure (P > 1 GPa) are less peralkaline (Aluminium Saturation Index, ASI = 0.63 – 0.77) than the starting glass composition (ASI = 0.48-0.57) due to the preferential partitioning of Na and K into the fluid compared to Al (Anderson and Burnham, 1983). The water contents of the haplogranite melts were calculated from the H_2O solubility model for peralkaline aluminosilicate melts calibrated by Mysen and Wheeler (2000) from 1000 to 1300 °C and 0.8 to 2 GPa. Using the temperature dependence of Mysen and Wheeler's data for NS4A6 compositions (6 mol% Al_2O_3, NBO/T = 0.17), which closely relates to the haplogranite melt used here (Table 1), the amount of water dissolved in the melt ranges between 3.0 ± 0.2 and 33.1 ± 5.0 wt% at the experimental conditions (Table 2).

The aqueous fluid and hydrous melt compositions were then used to determine their density. The density of the aqueous fluid phase was approximated to that of a NaCl aqueous solution with equivalent concentration in dissolved silicates using the equation of state of Driesner and Heinrich (2007) and Mantegazzi et al. (2013) at pressure below and above 0.6 GPa, respectively. The density of hydrous melts with variable water contents was determined at high P-T conditions using the equation of state determined by Malfait et al. (**2014**) for high P-T haplogranite melts with similar composition. Additional calculations were also performed to take into account the possible deviation of fluid and melt density induced by 1) changes on fluid composition with increasing temperature from a highly peralkaline to a more peraluminous composition (Anderson and Burnham, 1983; Manning et al., 2010) and 2) the effect of F on fluid composition and melt density (Dingwell et al., 1993; Webster, 1990). Consequently, the density of the high P-T aqueous fluids and hydrous melt varies between 0.58 ± 0.03 and 1.50 ± 0.21 g/cm^3, and 1.98 ±0.05 to 2.26 ±0.01 g/cm^3, respectively (Table 2). The uncertainties on the ρ_m/ρ_f

ratio are within 6 %, except at 700 °C and 2.4 GPa, where the significantly larger uncertainty on the determination of the aqueous fluid composition translates into a maximum uncertainty of 15 %.

The effective transmission through the fluid and melt, $\mathbf{T^{f}_{eff}}$ **and** $\mathbf{T^{m}_{eff}}$, represents the probability that the incoming X-ray excites a sample volume at depth x and the probability that the fluorescence radiation emitted by the sample volume traverses the samples without being absorbed. The effective transmission is then calculated as the average of $e^{-\mu_0 * x} * e^{-\mu_1 * (d-x)}$ over the entire sample thickness. μ_0 and μ_1 are respectively the absorption coefficient of the sample at the incident energy E_0 (18.05 keV) and at the energy of the characteristic fluorescence emission (Zr K-edge = 15.77 keV) derived as a function of melt or fluid compositions and densities using the Hephaestus software (Ravel and Newville, 2005). The sample thickness *d* was input as an average of the thickness of the sample chamber after each run (~ 200 μm). It may be noticed that uncertainties associated to samples thickness have a minor effect on $\mathbf{T^{m}_{eff}}$ **and** $\mathbf{T^{f}_{eff}}$, compared to other sources of uncertainty (*i.e.,* fluid and melt composition and density). A variation of the sample thickness by 50 μm, for instances, changes $\mathbf{T^{m}_{eff}}$ **and** $\mathbf{T^{f}_{eff}}$, by less than 1.1 and 4.4 %, respectively, and the total uncertainty on the $\mathbf{T^{m}_{eff}}$ **/** $\mathbf{T^{f}_{eff}}$ ratio remains within 4 %.

Over-all, the recourse to previous studies to constrain the composition, density and effective transmissions of the high P-T aqueous fluids and haplogranite melts translates into estimated uncertainties on the partition coefficients that do not exceed 16 %. The relatively modest uncertainty on the partition coefficient validates the experimental approach that permits *in situ* sampling of both the aqueous fluid and the hydrous melt and overcomes the need for calibration of the absolute fluorescence signal, the use an internal standard to calibrate Zr

296 concentrations or to determine the Zr concentrations in *post-mortem* analysis of the quenched
297 hydrous melts.
298

299 3. RESULTS AND DISCUSSION

300 The partition coefficients $D_{Zr}^{f/m}$ obtained from 575 to 800 °C and 0.3 to 2.4 GPa in Runs 1 to 3
301 are reported in Table 2. The evolution of $D_{Zr}^{f/m}$ in F-free and F-bearing systems are reported as a
302 function of temperature and water density in Fig. 4.
303

304 *The haplogranite-H_2O system*

305 In the haplogranite-H_2O system (Run 1 and 2), $D_{Zr}^{f/m}$ ranges from 0.19 ± 0.02 at 575 °C
306 and 0.7 GPa to 0.38 ± 0.03 at 745 °C and 1.5 GPa. There is however no significant effect of P-T
307 conditions on Zr partition coefficients, with a near constant $D_{Zr}^{f/m}$ within each separate run (Fig.
308 4.). This may result from the relatively low amounts of silicates dissolved in the aqueous fluids
309 within the investigated P-T range (< 15 wt%) and from the progressive increase of the Al
310 fraction in the fluid upon increasing pressure (Anderson and Burnham, 1983; Wohlers et al.,
311 2011) that hinder the formation of alkali-zirconosilicate complexes that are necessary to stabilize
312 significant amounts of Zr in the aqueous fluids (Louvel et al., 2013; Wilke et al., 2012).
313 Moreover, the $D_{Zr}^{f/m}$ determined in Run 1 (X_g = 0.79) are slightly larger than those determined in
314 Run 2 (X_g = 0.69) at similar P-T conditions, suggesting an increase of the partition coefficient
315 with increasing initial glass fraction (X_g) in the system (Fig. 4 - Table 2). Mysen and Armstrong
316 (2002) reported the increase of the Na dissolved in the fluid and a shift of the melt chemistry
317 towards a less peralkaline composition with increasing X_g above 0.5-0.6 in non-buffered alkali-

aluminosilicate systems. Such increase of the Na concentration in the fluid at expenses of the melt phase that evolves towards a less peralkaline composition could contribute to the increase of $D_{Zr}^{f/m}$ by promoting the formation of alkali-zirconosilicate complexes Zr-O-Si/Na in the aqueous fluids (Wilke et al., 2012; Louvel et al., 2013) while decreasing the stability of Zr in the silicate melt (Linnen and Keppler, 2002). These observations point towards a significant control of the fluid and melt composition and, particularly, of the alkalis to aluminum ratio ((Na+K)/Al) of each phase on Zr partitioning. This is consistent with a recent study reporting the decrease of zircon solubility with the addition of Al_2O_3 to alkali-silica aqueous fluids (Wilke et al., 2012).

The haplogranite-F-H_2O system

In the haplogranite-(F)-H_2O system (Run 3), the partitioning of Zr is significantly affected by P-T conditions (Table 2 and Fig. 4). The partition coefficient determined at 700 °C and 2.4 GPa falls within the range of values derived for the F-free system ($D_{Zr}^{f/m}$ = 0.32 ±0.04). This observation leads to the conclusion that neither the P-T conditions nor the presence of F significantly affect the partitioning of Zr between the fluid and melt at high pressure conditions. We note however a dramatic increase of the $D_{Zr}^{f/m}$ to 1.40 ± 0.10 at 800 °C and 0.3 GPa, indicating that Zr partitions strongly in favor of the aqueous phase. Interestingly, Webster et al. (1989) observed a similar enrichment in Nb in aqueous fluids coexisting with F- (and Cl-) bearing **metaluminous** granitic melts at temperature above 850 °C at 0.2 GPa (Fig. 5). The reverse partitioning of HFSE (Zr and Nb) into the aqueous phase at high temperatures (T > 800 °C) observed in Webster's and our study **involving peralkaline compositions** contrast with the behavior reported at lower temperatures in a similar pressure range, where $D_{Zr,Nb}^{f/m}$ remains lower

than 1 (London et al., 1988; Webster et al., 1989). We note however that the Nb partition coefficients by Borodulin et al. (2009) at 0.1 GPa are 1-2 orders of magnitude smaller ($D_{Nb}^{f/m}$ = 0.001-0.02) than the results from London et al. (1988) and Webster et al. (1989) even at temperatures above > 800 °C. The extremely low $D_{Nb}^{f/m}$ values of Borodulin et al. (2009) may be likely associated to an underestimation of Nb in analysis of **recovered** fluids by ICP-MS or ICP-AES analysis. Combined with the data of London et al. (1988), our experimental results display a similar trend than the Nb data of Webster et al. (1989), with an increase of $D_{Zr}^{f/m}$ above 1 as temperature increases from 650 to 800 °C at P ≤ 0.3 GPa (Fig. 5). **A direct comparison between the available datasets may appear unwarranted due to differences in the melt composition (peralkaline vs. metaluminous), water contents and degree of polymerization. However, while the peralkalinity index of the melt is expected to affect the absolute value of the partition coefficients (Borodulin et al., 2009), the observed trend with temperature is likely to be maintained.** Our data further suggest that the addition of chlorine is not necessary to favour Zr (or HFSE) partitioning towards the aqueous fluid as suggested by Webster et al. (1989). **We emphasize that the observations reported above are based on a relatively few Zr and Nb fluid/melt partitioning data and that systematic studies of the effect of fluid and melt composition of the partitioning will be required before more robust conclusions can be drawn.**

The large effect of temperature on Zr and Nb partitioning in F-bearing fluid/melt systems at low pressures (**Fig. 5**) raises questions regarding the mechanisms controlling HFSE incorporation in aqueous fluids in F-bearing systems. The formation of HFSE-F complexes is primarily quoted to explain the enhanced solubility of HFSE in F-bearing fluids or melts (Keppler, 1993; Migdisov et al., 2011; Rapp et al., 2010) and could plausibly account for the

363 preferential partitioning of HFSE towards the aqueous fluids observed in Webster's et al. (1989)
364 and our study. Although molecular dynamic (MD) simulations suggest the formation of hydrated
365 TiF species in Ti-bearing high P-T aqueous fluids (van Sijl, 2011), spectroscopic studies have
366 not yet provided conclusive evidences for HFSE-F complexation in silicate melts or alkali-silica
367 rich aqueous fluids (Farges, 1996; Louvel et al., 2013). Nevertheless, the low F content in our
368 experimental fluids (ca. 0.4 wt% F), resulting for the preferential partitioning of F into the
369 hydrous melt (Webster, 1990), suggests that HFSE-F complexation is not extensive in the fluid
370 and may not be sufficient to explain the favorable partitioning of Zr into the fluid at low pressure
371 and high temperature. Alternatively, the partitioning of Zr and Nb into the aqueous fluid at low
372 pressure **– high temperature** could be associated to an increase in the peralkalinity of the fluid
373 with temperature. Anderson and Burnham (1983) showed that low pressure (< 0.4 GPa) aqueous
374 fluids in equilibrium with albite progressively evolve towards more peralkaline compositions
375 with increasing temperature. This result, together with the increased capacity of F-bearing fluids
376 to dissolved higher amounts of silicate species (Si, Na and Al) than pure H_2O (Webster, 1990),
377 indicates that the experimental fluid phase at 800 °C and 0.3 GPa will be enriched in dissolved
378 silicates and highly peralkaline. As a result, the composition of the co-existing hydrous
379 haplogranite melt will be significantly less peralkaline compared to the experiments conducted at
380 higher pressure. Such modification of the fluid and melt compositions could both decrease the
381 solubility of HFSE in the silicate melt (Dickinson and Hess, 1985; Linnen and Keppler, 1997-
382 2002) and favor the formation of alkali-zirconosilicate complexes similar to those observed in Si,
383 Na-rich fluids and hydrous melts (Louvel et al., 2013) in the aqueous phase, hence promoting the
384 partitioning of HFSE into the fluid.

It is interesting to note that higher temperatures are apparently necessary to favour Nb partition into the low pressure fluids, although both elements display similar partitioning trends upon increasing temperature (Fig. 5.). Because Zr and Nb diplay similarities in their coordination environment in both diluted aqueous fluids and hydrous silicate melts (Louvel et al., 2013; Mayanovic et al., 2007), the stronger affinity of Zr for the aqueous fluid may thus denote an influence of the ionic charge on the solubility mechanism. It is thus plausible that the formation of the 6-coordinated alkali-niobiosilicate NbO_6-Si/Na clusters, which favor the incorporation of Nb^{5+} in the aqueous fluid, requires higher solute concentrations than necessary to stabilize alkali-zirconosilicate ZrO_6-Si/Na clusters.

4. GEOCHEMICAL IMPLICATIONS

4.1. Mobilization of HFSE in subduction zones

The fluid-melt partition coefficients for Zr determined in this study at P-T conditions relevant for the release of aqueous fluids and hydrous melts from the subducting slab (T > 500 °C and P > 1 GPa – Hermann et al., 2006; Manning, 2004; Schmidt and Poli, 1998; Spandler and Hermann; 2008) are systematically higher than 0.1, both in F-free and F-bearing systems. Although Zr preferentially partitions into hydrous silicate melts at these conditions, the relatively high $D_{Zr}^{f/m}$ values provide evidence for the incorporation of non-negligible amounts of this nominally insoluble element into the aqueous fluid phase. These results hence support that not only slab melts but also water-rich phases containing dissolved alkali-silicate species as those produced by metamorphic dehydration reactions may be important vectors for the transfer of Zr from the slab to the mantle wedge. **A quantitative estimate of the uptake of Zr by**

dehydration fluids would require Zr partition coefficients between typical slab minerals (*i.e.*, garnet, pyroxenes or amphiboles) and the aqueous fluid phase that remain scarce and limited to temperatures above 1200 °C (Ayers et al., 1997; Kessel et al., 2005; Stalder et al., 1998). Moreover, the aqueous fluid-melt partitioning coefficients in this study were determined at temperatures below the range where crystal- melt partitioning $D_{Zr}^{c/m}$ data is available, hence limiting the indirect evaluation of crystal-fluid partition coefficients $D_{Zr}^{c/f}$ ($D_{Zr}^{c/f} = D_{Zr}^{c/m}/D_{Zr}^{f/m}$). Nevertheless, mineral-melt partition coefficients reported for various silicic melts between 1 and 4 GPa at temperatures below 1200 °C are systematically smaller than 0.1 for orthopyroxenes, close to 0.1 for clinopyroxenes and greater than 0.1 for garnet (Adam and Green, 2006; Green et al., 2000; Huang et al., 2006). Thus, Zr may preferentially partition from the fluid phase into garnet and probably clinopyroxenes, but not into orthopyroxenes. Such **qualitative behavior of Zr during fluid-rock interactions** and the affinities are consistent with available $D_{Zr}^{c/f}$ reported by experiments conducted at higher P-T conditions (Ayers et al., 1997; Kessel et al., 2005; Stalder et al., 1998) **and will control the segregation of Zr into refractory phases in the slab.**

Similarities between the solubility behavior of columbite ($MnNb_2O_6$), rutile (TiO_2) and zircon ($ZrSiO_4$) in silicate melts and aqueous fluids (Dickinson and Hess, 1985; Linnen and Keppler, 1997; Linnen and Keppler, 2002; Manning et al., 2008) suggest that Ti and Nb should also be efficiently mobilized by the slab flux, regardless of their nature (aqueous fluid, hydrous melt or supercritical liquid). **The picture that emerges from these series of experimental studies is that melting of the slab is not necessary to mobilize HFSE in subduction zones and that aqueous fluids may contribute significantly to their recycling in subduction zones. Thus, the typical HFSE depletion recorded in most arc magmas may arise from fluid-rock**

interactions during fluid migration through the slab interface and mantle wedge, rather than from HFSE low solubility in slab-derived aqueous phases. Fluid reactions with mantle wedge peridotite may indeed trigger the precipitation of the slab-derived solutes (Manning 2004a; Hack and Thompson 2011) and favor HFSE segregation into refractory mineral phases (e.g., garnet, rutile or clinopyroxene, - Hermann and Spandler, 2008; Hermann and Rubatto, 2009; Johnson and Plank, 1999; Kessel et al., 2005; Klemme et al., 2002-2005). While dehydration-hydration processes could remobilize HFSE **in the mantle wedge**, it is likely that the hydrated peridotites adjacent to the top of the slab are ultimately recycled down to the transition zone with the subducting slab (Schmidt and Poli, 1998), **further** preventing HFSE from reaching the source of arc magmas. The HFSE enrichment recorded in high-Nb basalts (HNB) or adakitic magmas (Aguillon-Robles et al., 2001; Defant and Drummond, 1993, Munker et al., 2004) may thus arise from a combination of particular slab composition, subduction zone geometry and geothermal gradients that enable particular flow paths and/or significantly larger production of slab-derived fluids that could progressively consume the HFSE-bearing phases and ultimately lead to the recycling of HFSE up to the volcanic arc.

4.2. HFSE enrichment in shallow magmatic-hydrothermal environments

In large crustal granitic complexes, the intrusion of alkaline halogen-rich magmatic bodies can lead to the formation of rare metals (Zr, Nb, REE) ore deposits (*e.g.,* Strange Lake and Thor Lake Nechalacho deposit, Canada; Galineiro complex, Spain). The formation of HFSE-rich aggregates has often been considered as the result of the incompatible behaviour of HFSE during fractional crystallization (Boily and Williams-Jones, 1994). However, petrological and geochemical field observations, as well as numerical studies of fluid reaction paths indicate that

454 the exsolution of highly alkaline late-magmatic fluids from crystallizing F-rich intrusions at T <
455 600 °C enhance the remobilization of HFSE and the potential to form economical rare metal ore
456 deposits (Agangi et al., 2010; Gysi and Williams-Jones, 2013; **Montero et al., 1998;** Salvi and
457 Williams-Jones, 1996; Schaltegger, 2007; Sheard et al., 2012). The positive $D^{f/m}$ reported in
458 this study for Zr and previously for Nb (Webster et al., 1989) at low pressures and temperatures
459 above 800 °C in related chemical systems suggests that similar processes could also occur at
460 higher temperature in the earlier stages of the magmatic evolution. The exsolution of high-
461 temperature alkaline fluids at pressures below 0.4 GPa have thus the potential to extract HFSE
462 from F-rich granitic melt and may play a significant role in the formation of rare metal ore
463 deposits. Although such deposits have not been described in subduction-related environment, the
464 occurrence of HFSE-bearing accessory phases in volcanic vesicles at Lewotolo volcano
465 (Indonesia), or the record of noticeable HFSE scavenging at the Los Azufres geothermal field
466 (Mexico) provide evidences for the volatile-induced transport of HFSE in volcanic arcs (de Hoog
467 and van Bergen, 2000; Torres-Alvarado et al., 2007). The **potential** mobilization and
468 redistribution of HFSE by high temperature-low pressure **(T > 700 – 800 °C; 0.05 < P < 0.3**
469 **GPa)** fluids and vapors in volcanic arcs **could have** critical implications for the geochemical
470 interpretation of the trace element signature of arc magmas and will require further detailed
471 experimental investigations.
472
473 **Acknowledgements:** We would like to thank O. Proux for assistance during the synchrotron
474 experiments and M. Wälle for help with the LA-ICMPS analyses in quenched melts. A.B.
475 Thompson and C. Manning are acknowledged for helpful comments on a preliminary version of
476 the manuscript. The ESRF is acknowledged for provision of beamtime for these experiments.

This work was supported by the Swiss National Science Foundation through grants SNF 200021-120575 and SNF 200020-132208 to CSV.

REFERENCES CITED

Adam, J. and Green, T. H. (2006) Trace element partitioning between mica- and amphibole-bearing garnet lherzolite and hydrous basanitic melt: 1. Experimental results and the investigation of controls on partitioning behaviour. Contributions to Mineralogy and Petrology 152, 1-17.

Adam, J., Green, T. H., Sie, S. H. and Ryan, C. G. (1997) Trace element partitioning between aqueous fluids, silicate melts and minerals. European Journal of Mineralogy 9, 569-584.

Agangi, A., Kamenetsky, V. S., and McPhie, J. (2010) The role of fluorine in the concentration and transport of lithophile trace elements in felsic magmas: Insights from the Gawler Range Volcanics, South Australia. Chemical Geology 273, 314-325.

Aguillon-Robles, A., Calmus, T., Benoit, M., Bellon, H., Maury, R. O., Cotten, J., Bourgois, J., and Michaud, F. (2001) Late miocene adakites and Nb-enriched basalts from Vizcaino Peninsula, Mexico: Indicators of East Pacific Rise subduction below Southern Baja California? Geology 29, 531-534.

Anderson, G. M. and Burnham, C. W.(1983) Feldspar solubility and the transport of aluminum under metamorphic conditions. American Journal of Science 283, 283-297.

Antignano, A. and Manning, C. E.(2008) Rutile solubility in H_2O, H_2O-SiO_2, and H_2O-$NaAlSi_3O_8$ fluids at 0.7-2.0 GPa and 700-1000 °C: Implications for mobility of nominally insoluble elements. Chemical Geology 255, 283-293.

Audetat, A. and Keppler, H. (2005) Solubility of rutile in subduction zone fluids, as determined by experiments in the hydrothermal diamond anvil cell. Earth and Planetary Science Letters 232, 393-402.

501 Ayers, J. C., Dittmer, S. K. and Layne, G. D. (1997) Partitioning of elements between peridotite and H_2O
502 at 2.0-3.0 GPa and 900-1000 °C, and application to models of subduction zone processes. Earth
503 and Planetary Science Letters 150, 381-398.
504 Bassett, W. A., Shen, A. H., Bucknum, M., and Chou, I. M. (1993) A New Diamond-Anvil Cell for
505 Hydrothermal Studies to 2.5 GPa and from -190 °C to 1200 °C. Review of Scientific Instruments
506 64, 2340-2345.
507 Bassett, W. A., Anderson, A. J., Mayanovic, R. A. and Chou, I. M. (2000) Hydrothermal diamond anvil
508 cell for XAFS studies of first-row transition elements in aqueous solution up to supercritical
509 conditions. Chemical Geology 167, 3-10.
510 Borchert, M., Wilke, M., Schmidt, C., and Rickers, K. (2009) Partitioning and equilibration of Rb and Sr
511 between silicate melts and aqueous fluids. Chemical Geology 259, 39-47.
512 Borodulin, G. P., Chevychelov, V. Y., and Zaraysky, G. P. (2009) Experimental study of partitioning of
513 tantalum, niobium, manganese, and fluorine between aqueous fluoride fluid and granitic and
514 alkaline melts. Doklady Earth Sciences 427, 868-873.
515 Bouvier, A-S., Deloule, E. and Metrich, A. (2010) Fluid inputs to magma sources of St. Vincent and
516 Grenada (Lesser Antilles): New insights from trace elements in olivine-hosted melt inclusions.
517 Journal of Petrology 51, 1597-1615.
518 Boily, M. and Williams-Jones, A. E. (1994) The role of magmatic and hydrothermal processes in the
519 chemical evolution of the Strange Lake plutonic complex, Quebec-Labrador. Contributions to
520 Mineralogy and Petrology 118, 33-47.
521 Brenan, J. M., Shaw, H. F., Phinney, D. L., and Ryerson, F. J. (1994) Rutile-aqueous fluid partitioning of
522 Nb, Ta, Hf, Zr, U and Th - Implications for High-Field Strength Element depletion in island-arc
523 basalts. Earth and Planetary Science Letters 128, 327-339.
524 Bureau, H. and Keppler, H. (1999) Complete miscibility between silicate melts and hydrous fluids in the
525 upper mantle: experimental evidence and geochemical implications. Earth and Planetary Science
526 Letters 165, 187-196.

Cauzid, J., Philippot, P., Somogyi, A., Menez, B., Simionovici, A., and Bleuet, P. (2006) Standardless quantification of single fluid inclusions using synchrotron radiation induced X-ray fluorescence. Chemical Geology 227, 165-183.

Defant, M. J. and Drummond, M. S. (1993) Mount St-Helens: Potential example of the partial melting of the subducted lithosphere in a volcanic arc. Geology 21, 547-550.

Dickinson, J. E. and Hess, P. C., 1985. Rutile solubility and Titanium coordination in silicate melts. Geochimica Et Cosmochimica Acta 49, 2289-2296.

Dingwell, D. B., Knoche, R., and Webb, S. L. (1993) The effect of F on the density of haplogranite melt. American Mineralogist 78, 325-330.

Driesner, T. and Heinrich, C. A. (2007) The system H_2O-NaCl. Part I: Correlation formulae for phase relations in temperature-pressure-composition space from 0 to 1000 degrees °C, 0 to 5000 bar, and 0 to 1 X-NaCl. Geochimica Et Cosmochimica Acta 71, 4880-4901.

Farges, F. (1996) Does Zr-F "complexation" occur in magmas? Chemical Geology 127, 253-268.

Foley, S. F., Barth, M. G., and Jenner, G. A. (2000) Rutile/melt partition coefficients for trace elements and an assessment of the influence of rutile on the trace element characteristics of subduction zone magmas. Geochimica Et Cosmochimica Acta 64, 933-938.

Gao, J., John, T., Klemd, R., and Xiong, X. M. (2007) Mobilization of Ti-Nb-Ta during subduction: Evidence from rutile-bearing dehydration segregations and veins hosted in eclogite, Tianshan, NW China. Geochimica Et Cosmochimica Acta 71, 4974-4996.

Gill, J. B. (1981) Orogenic andesites and plate tectonics. Springer-Verlag, pp 390.

Green, T. H., Blundy, J. D., Adam., J. and Yaxley, G. M. (2000) SIMS determination of trace element partition coefficients between garnet, clinopyroxene and hydrous basaltic liquids at 2-7.5 GPa and 1080-1200 °C. Lithos 53, 165-187.

Gysi, A. P. and Williams-Jones, A. E. (2013) Hydrothermal mobilization of pegmatite-hosted REE and Zr at Strange Lake, Canada: A reaction path model. Geochimica et Cosmochimica Acta 122, 324-352.

552 Hack, A. C. and Thompson, A. B. (2011) Density and Viscosity of Hydrous Magmas and Related Fluids
553 and their Role in Subduction Zone Processes. Journal of Petrology 52, 1333-1362.
554 Hawkesworth, C. J., Hergt, J. M., Ellam, R. M., and McDermott, F. (1991) Element fluxes associated
555 with subduction-related magmatism. Philosophical Transactions of the Royal Society of London
556 Series a-Mathematical Physical and Engineering Sciences 335, 393-405.
557 Hayden, L. A. and Manning, C. E. (2011) Rutile solubility in supercritical $NaAlSi_3O_8$-H_2O fluids.
558 Chemical Geology 284, 74-81.
559 Hermann, J., and Spandler, C. (2008) Sediment melts at sub-arc depths: an Experimental Study. Journal
560 of Petrology 49, 717-740.
561 Hermann J., and Rubatto, D. (2009) Accessory phase control on the trace element signature of sediment
562 melts in subduction zones. Chemical Geology 265, 512-526.
563 Hermann, J., Spandler, C., Hack, A., and Korsakov, A. V. (2006) Aqueous fluids and hydrous melts in
564 high-pressure and ultra-high pressure rocks: Implications for element transfer in subduction zones.
565 Lithos 92, 399-417.
566 Huang, F., Lundstrom, C. C. and McDonough, W. F. (2006) Effect of melt structure on trace-element
567 partitioning between clinopyroxene and silicic, alkaline, aluminous melts. American Mineralogist
568 91, 1385-1400.
569 Jamieson, J. C., Fritz, J. N., and Manghnani, M. H. (1982) Pressure measurement at high temperature in
570 X-ray diffraction studies: gold as a primary standard *in* High-Pressure Research in Geophysics. S.
571 Akimoto and M.H. Manghnani (Ed.) pp 27-48. Center for Academic Publishing, Tokyo.
572 Johnson, M. C., and Plank, T. (1999) Dehydration and melting experiments constrain the fate of
573 subducted sediments. Geochemistry, Geophysics, Geosystems 1, 1-26.
574 Kelemen, P. B., Johnson, K. T. M., Kinzler, R. J., and Irving, A. J. (1990) High Field Strength Element
575 depletions in acr basalts due to mantle-magma interactions. Nature 345, 521-524.
576 Keppler, H. (1993) Influence of Fluorine on the Enrichment of High-Field Strength Trace-Elements in
577 Granitic-Rocks. Contributions to Mineralogy and Petrology 114, 479-488.

578 Keppler, H. (1996) Constraints from partitioning experiments on the composition of subduction-zone
579 fluids. Nature 380, 237-240.
580 Kessel, R., Schmidt, M. W., Ulmer, P., and Pettke, T. (2005) Trace element signature of subduction-zone
581 fluids, melts and supercritical liquids at 120-180 km depth. Nature 437, 724-727.
582 Klemme, S., Blundy, J.D. and Wood, B.J. (2002) Experimental constraints on major and trace element
583 partitioning during partial melting of eclogite. Geochimica et Cosmochimica Acta 66, 3109-3023.
584 Klemme, S., Prowatke, S., Hametner, K., and Gunther, D. (2005) Partitioning of trace elements between
585 rutile and silicate melts: Implications for subduction zones. Geochimica Et Cosmochimica Acta 69,
586 2361-2371.
587 Klimm, K., Blundy, J.D. and Green, H. (2008) Trace element partitioning and accessory phase saturation
588 during H_2O-saturated melting of basalt with implications for subduction zone chemical fluxes.
589 Journal or Petrology 49, 523-553.
590 Linnen, R. L. and Keppler, H. (1997) Columbite solubility in granitic melts: consequences for the
591 enrichment and fractionation of Nb and Ta in the Earth's crust. Contributions to Mineralogy and
592 Petrology 128, 213-227.
593 Linnen, R. L. and Keppler, H. (2002) Melt composition control of Zr/Hf fractionation in magmatic
594 processes. Geochimica Et Cosmochimica Acta 66, 3293-3301.
595 London, D., Hervig, R. L., and Morgan, G. B. (1988) Melt-vapor solubilities and elemental partitioning in
596 peraluminous granite-pegmatite systems - Experimental results with Macusani glass at 200 MPa.
597 Contributions to Mineralogy and Petrology 99, 360-373.
598 Louvel, M., Sanchez-Valle, C., Malfait, W.J., Testemale, D. and Hazemann, J-L. (2013) Zr complexation
599 in high pressure fluids and implications for the mobilization of HFSE in subduction zones.
600 Geochimica et Cosmochimica Acta 104, 281-299.
601 Malfait, W.J., Seifert, R., Petitgirard, S., Perrillat, J-P., Mezouar, M., Ota, T., Nakamura, E., Lerch, P. and
602 Sanchez-Valle, C. (2014) Supervolcano eruptions driven by melt buoyancy in large silicic magma
603 chambers. Nature Geosciences 7, 122-125.

Manning, C. E. (2004) The chemistry of subduction-zone fluids. Earth and Planetary Science Letters 223, 1-16.

Manning, C. E., Wilke, M., Schmidt, C., and Cauzid, J. (2008) Rutile solubility in albite-H_2O and $Na_2Si_3O_7$-H_2O at high temperatures and pressures by in-situ synchrotron radiation micro-XRF. Earth and Planetary Science Letters 272, 730-737.

Manning, C. E., Antignano, A., and Lin, H. A. (2010) Premelting polymerization of crustal and mantle fluids, as indicated by the solubility of albite plus paragonite plus quartz in H_2O at 1 GPa and 350-620 °C. Earth and Planetary Science Letters 292, 325-336.

Mantegazzi, D., Sanchez-Valle, C. and Driesner, T. (2013) Thermodynamic properties of aqueous NaCl solutions to 1073K and 4.5 GPa, and implications for dehydration reaction in subducting slabs. Geochimica et Cosmochimica Acta 121, 263-290.

Mayanovic, R. A., Anderson, A.J., Bassett, W.A. and Chou, I-M., 2007. Synchrotron x-ray spectroscopy of Eu/HNO3 aqueous solutions at high temperatures and pressure and Nb-bearing silicate melt phases coexisting with hydrothermal fluids using a modified hydrothermal diamond anvil cell and rail assembly. Review of Scientific Instruments 78, 053904,1-9.

Mibe, K., Chou, I-M. and Bassett, W. A. (2008) In situ Raman spectroscopic investigation of the structure of subduction-zone fluids. Journal of Geophysical Research 11, B04208-1-8.

Migdisov, A. A., Williams-Jones, A. E., van Hinsberg, V., and Salvi, S. (2011) An experimental study of the solubility of baddeleyite (ZrO_2) in fluoride-bearing solutions at elevated temperature. Geochimica Et Cosmochimica Acta 75, 7426–7434.

Montero, P., Floor, P and Corretge, G., 1998. The accumulation of rare-earth and high-field-strength elements in peralkaline granitic rocks: The Galineiro orthogneissic complex, Northwestern Spain. The Canadian Mineralogist 36, 683-700.

628 Munker, C., Worner, G., Yogodzinski, G., and Churikova, T. (2004) Behaviour of high field strength
629 elements in subduction zones: constraints from Kamchatka-Aleutian arc lavas. Earth and Planetary
630 Science Letters 224, 275-293.
631 Mysen, B. O. and Wheeler, K. (2000) Solubility behavior of water in haploandesitic melts at high
632 pressure and high temperature. American Mineralogist 85, 1128-1142.
633 **Prouteau, G., Scaillet, B., Pichavant, M. and Maury, R., 2001. Evidence for mantle metasomatism**
634 **by hydrous silicic melts derived from subducted oceanic crust. Nature 410, 197-200.**
635 Proux, O., Biquard, X., Lahera, E., Menthonnex, J. J., Prat, A., Ulrich, O., Soldo, Y., Trevisson, P.,
636 Kapoujyan, G., Perroux, G., Taunier, P., Grand, D., Jeantet, P., Deleglise, M., Roux, J. P., and
637 Hazemann, J. L. (2005) FAME: A new beamline for X-ray absorption investigations of very diluted
638 systems of environmental, material and biological interests. Physica Scripta T115, 970-973.
639 Proux, O., Nassif, V., Prat, A., Ulrich, O., Lahera, E., Biquard, X., Menthonnex, J. J., and Hazemann, J.-
640 L. (2006) Feedback system of a liquid-nitrogen-cooled double-crystal monochromator: design and
641 performances. Journal of Synchrotron Radiation 13, 59-68.
642 Rapp, J. F., Klemme, S., Butler, I. B., and Harley, S. L. (2010) Extremely high solubility of rutile in
643 chloride and fluoride-bearing metamorphic fluids: An experimental investigation. Geology 38, 323-
644 326.
645 Ravel, B. and Newville, M. (2005) ATHENA, ARTEMIS, HEPHAESTUS: data analysis for X-ray
646 absorption spectroscopy using IFEFFIT. Journal of Synchrotron Radiation 12, 537-541.
647 Rubatto, D. and Hermann, J. (2003) Zircon formation during fluid circulation in eclogites (Monviso,
648 Western Alps): Implications for Zr and Hf budget in subduction zones. Geochimica Et
649 Cosmochimica Acta 67, 2173-2187.
650 Rudnick, R. L., Barth, M., Horn, I., and McDonough, W. F. (2000) Rutile-bearing refractory eclogites:
651 Missing link between continents and depleted mantle. Science 287, 278-281.

652 Salvi, S. and Williams-Jones, A. E. (1996) The role of hydrothermal processes in concentrating high-field
653 strength elements in the Strange Lake peralkaline complex, northeastern Canada. Geochimica Et
654 Cosmochimica Acta 60, 1917-1932.
655 Sanchez-Valle, C. (2013) Structure and thermodynamics of subduction zone fluids from spectroscopic
656 studies. Reviews in Mineralogy and Geochemistry 76, 265-309.
657 Sanchez-Valle, C., Martinez, I., Daniel, I., Philippot, P., Bohic, S., and Simionovici, A. (2003)
658 Dissolution of strontianite at high P-T conditions: An in-situ synchrotron X-ray fluorescence study.
659 American Mineralogist 88, 978-985.
660 Sanchez-Valle, C., Daniel, I., Martinez, I., Simionovici, A., and Reynard, B. (2004) Progress in
661 quantitative elemental analyses in high P-T fluids using synchrotron x-ray fluorescence (SXRF).
662 Journal of Physics: Condensed Matter 16, S1197-S1206.
663 Scambelluri, M. and Philippot, P. (2001) Deep fluids in subduction zones. Lithos 55, 213-227
664 Schaltegger, U. (2007) Hydrothermal zircon. Elements 3, 51-79.
665 Schmidt, M. W. and Poli, S. (1998) Experimentally based water budgets for dehydrating slabs and
666 consequences for arc magma generation. Earth and Planetary Science Letters 163, 361-379.
667 Sheard, E. R., Williams-Jones, A. E., Heiligmann, M., Pederson, C. and Trueman, D. L. (2012) Controls
668 on the Concentration of Zirconium, Niobium, and the Rare Earth Elements in the Thor Lake Rare
669 Metal Deposit, Northwest Territories, Canada. Economic Geology 107, 81-104.
670 Shen, A. and Keppler, H. (1995) Infrared spectroscopy of hydrous silicate melts to 1000 °C and 10 kbar:
671 Direct observation of H_2O speciation in a diamond-anvil cell. American Mineralogist 80, 1335-
672 1338.
673 Spandler, C., Mavrogenes, J. and Hermann, J. (2007) Experimental constraints on element mobility from
674 subducted sediments using high-P synthetic fluid/melt inclusions. Chemical Geology 239, 228-249.
675 Sparks, R. S. J. (1980) X-ray Fluorescence Microprobe for Chemical Analysis. Synchrotron Radiation
676 Research, Plenum Press, pp 754.

677 Stalder, R., Foley, S. F., Brey, G. P., and Horn, I.(1998) Mineral aqueous fluid partitioning of trace
678 elements at 900-1200 °C and 3.0-5.7 GPa: New experimental data for garnet, clinopyroxene, and
679 rutile, and implications for mantle metasomatism. Geochimica Et Cosmochimica Acta 62, 1781-
680 1801.
681 Stern, R. J. (2002) Subduction zones. Reviews of Geophysics 40 (4), 3-138.
682 Tropper, P. and Manning, C. E. (2005) Very low solubility of rutile in H_2O at high pressure and
683 temperature, and its implications for Ti mobility in subduction zones. American Mineralogist 90,
684 502-505.
685 van Sijl, J. (2011) Trace elements in high pressure and temperature fluids in subduction zones, VU
686 University Amsterdam.
687 Wagner, W. and Pruss, A. (2002) The IAPWS formulation 1995 for the thermodynamic properties of
688 ordinary water substance for general and scientific use. Journal of Physical and Chemical
689 Reference Data 31(2), 387-535.
690 Webster, J. D. (1990) Partitioning of F between H_2O and CO_2 fluids and topaz rhyolite melt -
691 Implications for mineralizing magmatic-hydrothermal fluids in F-rich granitic systems.
692 Contributions to Mineralogy and Petrology 104, 424-438.
693 Webster, J. D., Holloway, J. R., and Hervig, R. L. (1989) Partitioning of lithophile trace-elements
694 between H_2O and H_2O+CO_2 fluids and topaz rhyolite melt. Economic Geology 84, 116-134.
695 Wilke, M., Schmidt, C., Dubrail, J., Appel, K., Borchert, M., Kvashnina, K. and Manning, C.E. (2012)
696 Zircon solubility and zirconium complexation in $H_2O+Na_2O+SiO_2\pm Al_2O_3$ fluids at high pressure
697 and temperature. Earth and Planetary Science Letters, 15-25.
698 Wohlers, A., Manning, C. E., and Thompson, A. B. (2011) Experimental investigation of the solubility of
699 albite and jadeite in H_2O, with paragonite plus quartz at 500 and 600 °C, and 1-2.25 GPa.
700 Geochimica Et Cosmochimica Acta 75, 2924-2939.
701

List of Table and Figure captions

Table 1. Chemical composition (in wt %) of the F-free and F-bearing haplogranite glasses used as starting materials as determined from Electron Microprobe analysis (EMPA).

Table 2: Zirconium fluid-melt partition coefficient as a function of P-T conditions, fluid and melt compositions and densities.

Figure 1. (a) Microphotograph of the compression chamber showing the hydrous haplogranite melt coexisting with the aqueous fluid at 700 °C and 2.4 GPa and 2D-SXRF maps showing the distribution of Zr between the coexisting phases**.** (b) SXRF profiles collected at the same P-T conditions across the sample chamber following the trajectories 1 and 2. The plateau displayed by the fluorescence signal of the melt globule indicates that the melt globule bridges both diamonds and therefore the melt phase can be measured without contamination from the aqueous fluid. SXRF spectra were collected in both the hydrous melt and aqueous phases to determine the partitioning coefficient of Zr between the phases.

Figure 2. Schematic view of the beam path through the diamond anvils and the sample chamber for the SXRF analysis of the hydrous melt (a) and the aqueous fluid (b) at identical P-T condition. E_0 and I_0, and E_X and I_X are respectively the energy and intensity of the incident beam and the X-ray fluorescence signal emitted by the sample. β represents the angle between the incident X-ray beam and the position of the detector for the collection of the fluorescence signal.

725 **Figure 3.** Zr Kα fluorescence line (15.77 keV) from normalized SXRF spectra collected in
726 alkali-SiO_2 rich fluid (blue line) and water-saturated haplogranite melt (red line) equilibrated at
727 660 °C and 1.5 GPa (run 1). The dashed lines represent the background subtracted from the
728 spectra to determine the integrated intensity of the K_α fluorescence line of Zr in the fluid and
729 melt, I_f and I_m, respectively.
730
731 **Figure 4.** Evolution of Zr partition coefficient $D_{Zr}^{f/m}$ as a function of temperature (a) and H_2O
732 density (b) for different initial glass fraction Xg in the system. The reported uncertainties take
733 into account the uncertainties on pressure (10%) and on the determination of fluid and melt
734 composition and density. Water densities are calculated using the density relations for pure water
735 of Wagner and Pruss (2002) up to 1 GPa and Mantegazzi et al. (2013) at higher pressures.
736
737 **Figure 5.** Effect of temperature on the partition coefficients of Zr and Nb between aqueous fluid-
738 and haplogranitic melt in F-bearing systems at pressures below 0.3 GPa. The black arrows
739 highlight the change on Zr and Nb partitioning with increasing temperature at 0.2-0.3 GPa.

Table 1. Chemical composition (in wt %) of the F-free and F-bearing haplogranite glasses used as starting materials as determined from Electron Microprobe analysis (EMPA).

Composition	Synthesis conditions		SiO_2[a]	Al_2O_3[a]	Na_2O[a]	K_2O[a]	ZrO_2[a]	F[a]	Total	H_2O[b]	ASI[c]	NBO/T[d]
	T (°C)	P (GPa)										
Haplo4	1200	1.5	75.74	8.32	7.56	4.52	0.418	-	96.558	3	0.48	0.13
Haplo4-F	1200	1.5	76.34	8.04	5.77	4.1	0.389	1.89	96.529	3	0.57	0.09

[a]Average of 20 EMPA analyses performed on each glass composition. Standard deviations are < 0.1 wt% for Na_2O, Al_2O_3, K_2O and F, < 0.4 wt% for SiO_2 and < 0.05 wt% for ZrO_2.

[b]Nominal H_2O concentration.

[c] $ASI = \frac{Al_2O_3}{Na_2O + K_2O}$ in moles.

[d] $NBOT / T = \frac{Na + K + 4Zr - Al}{Al + Si}$ in moles.

Table 2: Zirconium fluid-melt partition coefficient as a function of P-T conditions, fluid and melt compositions and densities.

X_g [a]	T (°C)	P (GPa) [b]	H_2O dissolved in melt [c]	Melt density [d] ρ_m	Transmission in melt T_m	Silicates in fluid	Fluid density [h] ρ_f	Transmission in fluid T_f	I^f_{Zr} / I^m_{Zr}	$D^{f/m}_{Zr}$
Haplogranite - H_2O										
Run 1 0.79	660	1.5	17.3 ±2.3	2.14 ±0.02	0.84 ±0.01	12.4 ±2.2[f] -15.3 ±3.3[e]	1.18 ±0.02	0.97 <0.01	***0.24*** *±0.02*	***0.38*** *±0.03*
	745	0.7	6.4 ±0.7	2.24 ±0.01	0.81 <0.01	4.9 ±1.1[e]	0.91 ±0.04	0.98 <0.01	***0.18*** *±0.01*	***0.37*** *±0.02*
Run 2 0.69	575	0.85	9.0 ±1.1	2.22 ±0.01	0.82 <0.01	3.3 ±0.6[e]	1.00 ±0.03	0.97 <0.01	***0.10*** *±0.01*	***0.19*** *±0.02*
	675	1.4	15.6 ±2.1	2.15 ±0.02	0.84 ±0.01	11.4 ±2.2[f] -15.5 ±2.8[e]	1.15 ±0.02	0.97 <0.01	***0.12*** *±0.01*	***0.20*** *±0.02*
Haplogranite – (F) –H_2O										
Run 3 0.69	700	2.4	33.1 ±5.0	1.98 ±0.05	0.88 ±0.01	10.5 ±0.5[f]	1.50 ±0.21	0.94 ±0.03	***0.26*** *±0.01*	***0.32*** *±0.04*
	800	0.3	3.0 ±0.2	2.26 <0.01	0.80 <0.01	1.1 ±0.2[e] – 5[g]	0.58 ±0.03	0.99 <0.01	***0.45*** *±0.01*	***1.40*** *±0.10*

Notes:

[a] Initial glass fraction in the loading (wt ±0.02) calculated considering an uncertainty of 10% on volumetric proportions.

[b] Uncertainty on pressure is 10%.

[c] H_2O solubility (in wt%) in the haplogranite melt calculated from the solubility data of Mysen and Wheeler (2000b)

[d] Melt density (in g/cm^{-3}) calculated as a function of P-T conditions and melt composition according to Malfait et al. (2013).

[e] Silicate (SiO_2, Na_2O, Al_2O_3 and K_2O) solubility (in wt%) in the aqueous fluid coexisting with haplogranite melt calculated from the albite solubility data of Anderson and Burnham (1983).

[f] Silicate solubility in the aqueous fluid estimated from Wohlers et al. (2011) for P > 1 GPa.

[g] Silicate solubility in the aqueous fluid in the presence of F, as estimated following Webster (1990).

[h] Fluid density (in g/cm^3) calculated as a function of P-T conditions from the data of Mantegazzi et al. (2013) at P > 0.5 GPa and of Driesner and Heinrich (2007) at P < 0.5 GPa.

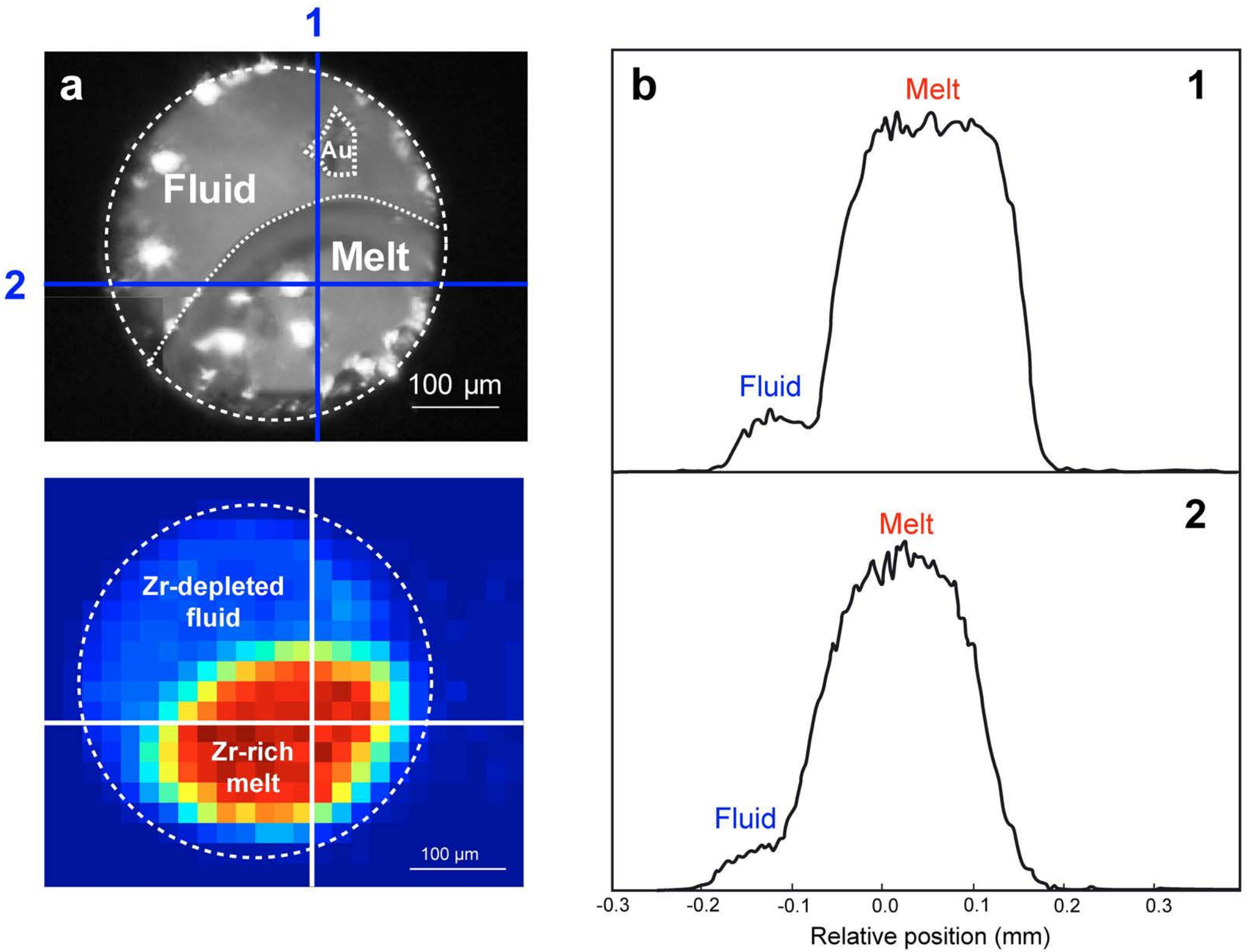
1
a
Au
Fluid
Melt
2
100 µm
Zr-depleted
fluid
Zr-rich
melt
100 µm
b
Melt
1
Fluid
Melt
2
Fluid
-0.3
-0.2
-0.1
0.0
0.1
0.2
0.3
Relative position (mm)

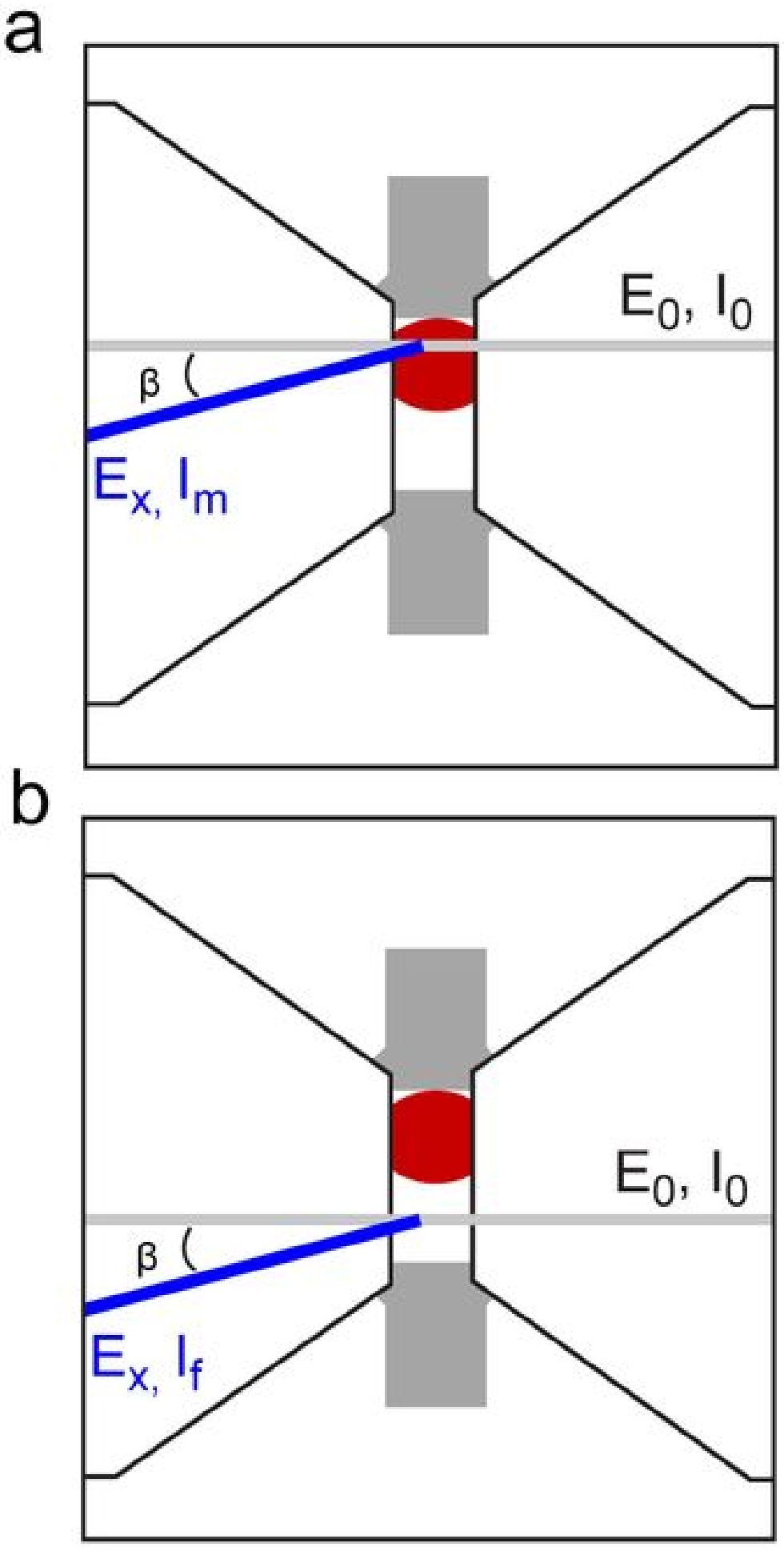
a
E_0, I_0
β (
E_x, I_m
b
E_0, I_0
β (
E_x, I_f

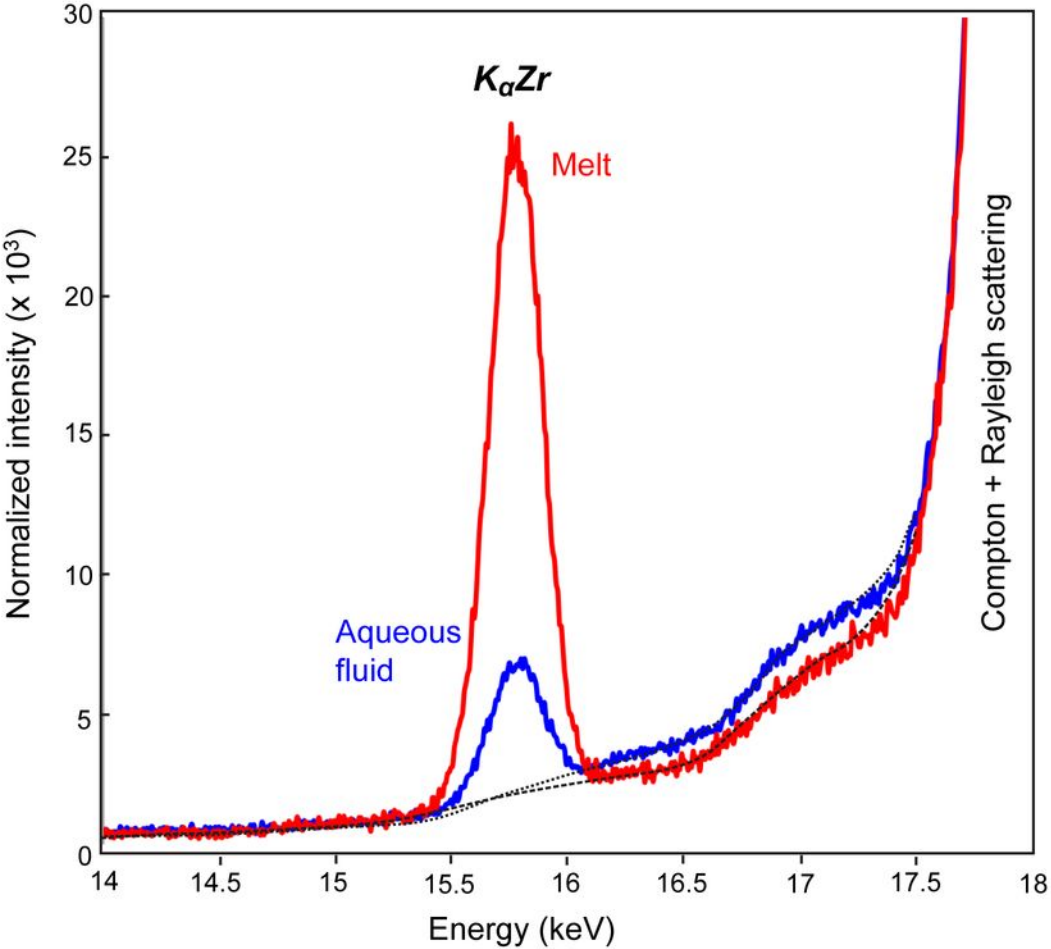
$K_\alpha Zr$
Melt
Aqueous fluid
Compton + Rayleigh scattering
Normalized intensity (x 10^3)
Energy (keV)
0
5
10
15
20
25
30
14
14.5
15
15.5
16
16.5
17
17.5
18

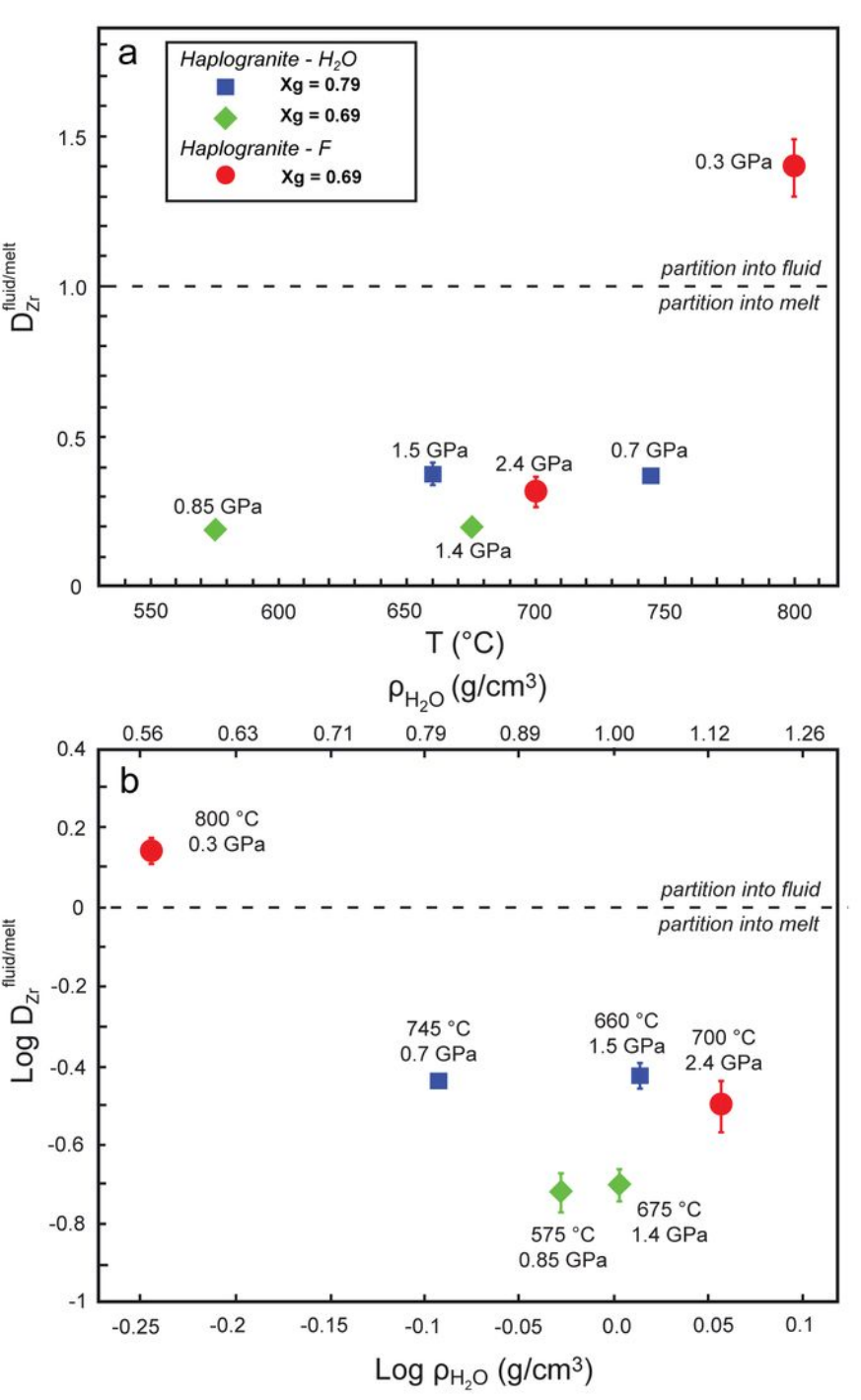
a
Haplogranite - H2O
Xg = 0.79
Xg = 0.69
Haplogranite - F
Xg = 0.69
0.3 GPa
partition into fluid
partition into melt
1.5 GPa
2.4 GPa
0.7 GPa
0.85 GPa
1.4 GPa
D Zr fluid/melt
T (°C)
ρ H2O (g/cm3)
b
800 °C
0.3 GPa
partition into fluid
partition into melt
745 °C
0.7 GPa
660 °C
1.5 GPa
700 °C
2.4 GPa
675 °C
1.4 GPa
575 °C
0.85 GPa
Log D Zr fluid/melt
Log ρ H2O (g/cm3)

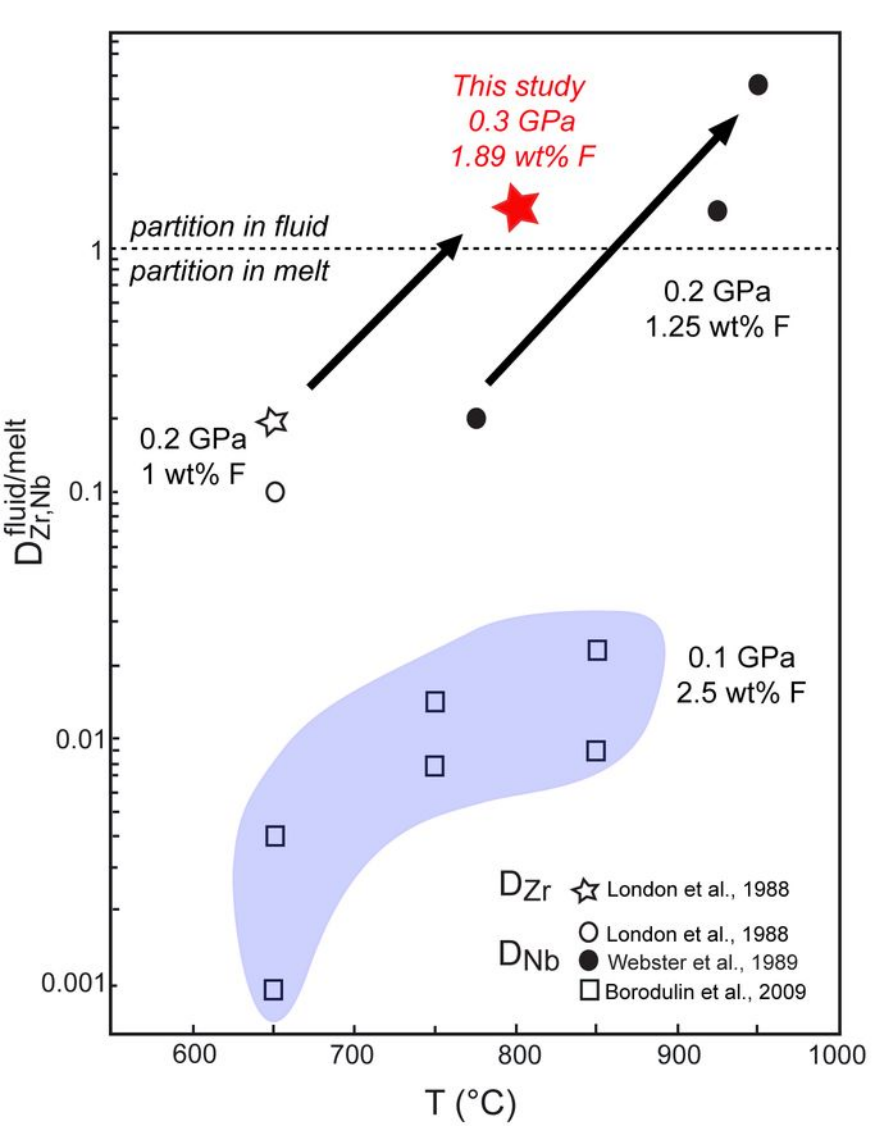
This study
0.3 GPa
1.89 wt% F
partition in fluid
partition in melt
1
0.2 GPa
1.25 wt% F
0.2 GPa
1 wt% F
0.1
0.1 GPa
2.5 wt% F
0.01
0.001
$D_{Zr,Nb}^{fluid/melt}$
D_{Zr} London et al., 1988
D_{Nb} London et al., 1988
Webster et al., 1989
Borodulin et al., 2009
600
700
800
900
1000
T (°C)